A compact incoherent broadband cavity-enhanced absorption spectrometer for trace detection of nitrogen oxides, iodine oxide and glyoxal at levels below parts per billion for field applications

Albane Barbero, Camille Blouzon, Joël E Savarino, Nicolas Caillon, Aurélien Dommergue, Roberto Grilli

Atmos. Meas. Tech., 13, 4317–4331, 2020
https://doi.org/10.5194/amt-13-4317-2020

Atmospheric Measurement Techniques
Open Access
EGU

A compact incoherent broadband cavity-enhanced absorption spectrometer for trace detection of nitrogen oxides, iodine oxide and glyoxal at levels below parts per billion for field applications

Albane Barbero, Camille Blouzon, Joël Savarino, Nicolas Caillon, Aurélien Dommergue, and Roberto Grilli

Université Grenoble Alpes, CNRS, IRD, Grenoble INP (Institute of Engineering, Université Grenoble Alpes), IGE, 38000 Grenoble, France

Correspondence: Roberto Grilli (roberto.grilli@cnrs.fr)

Received: 25 March 2020 – Discussion started: 2 April 2020
Revised: 9 July 2020 – Accepted: 14 July 2020 – Published: 17 August 2020

Abstract. We present a compact, affordable and robust instrument based on incoherent broadband cavity-enhanced absorption spectroscopy (IBBCEAS) for simultaneous detection of NO_x, IO, CHOCHO and O_3 in the 400–475 nm wavelength region. The instrument relies on the injection of a high-power LED source in a high-finesse cavity ($F \sim 33\,100$), with the transmission signal being detected by a compact spectrometer based on a high-order diffraction grating and a charge-coupled device (CCD) camera. A minimum detectable absorption of 2.0×10^{-10} cm^{-1} was achieved within ~ 22 min of total acquisition, corresponding to a figure of merit of 1.8×10^{-10} cm^{-1} Hz$^{-1/2}$ per spectral element. Due to the multiplexing broadband feature of the setup, multi-species detection can be performed with simultaneous detection of NO_2, IO, CHOCHO and O_3 achieving detection limits of 11, 0.3, 10 ppt (parts per trillion) and 47 ppb (parts per billion) (1σ) within 22 min of measurement, respectively (half of the time is spent on the acquisition of the reference spectrum in the absence of the absorber, and the other half is spent on the absorption spectrum). The implementation on the inlet gas line of a compact ozone generator based on electrolysis of water allows for the measurement of NO_x ($NO + NO_2$) and therefore an indirect detection of NO with detection limits for NO_x and NO of 10 and 21 ppt (1σ), respectively. The device has been designed to fit in a 19 in., 3U (5.25 in.) rack-mount case; weighs 15 kg; and has a total electrical power consumption of < 300 W. The instrument can be employed to address different scientific objectives such as better constraining the oxidative capacity of the atmosphere, studying the chemistry of highly reactive species in atmospheric chambers as well as in the field and looking at the sources of glyoxal in the marine boundary layer to study possible implications on the formation of secondary aerosol particles.

1 Introduction

Free radicals are controlling the oxidative capacity of the atmosphere and therefore contribute to the upholding of its chemical balance. With their unpaired valence electron, they are highly chemically reactive and are therefore considered the "detergents" of the atmosphere (Monks, 2005; Monks et al., 2009). Even if present at extremely low concentrations, radicals are constantly formed by photochemical and combustion processes. They may be removed from the atmosphere by biological uptakes, dry and wet deposition, and chemical reactions (Finlayson-Pitts and Pitts, 2000). Free radicals in the troposphere such as nitrogen oxides (NO_x), hydroxyl radical (OH), peroxy radicals (HO_2 and RO_2) and halogen oxides (BrO and IO) can be found at mixing ratios (i.e. mole fractions) ranging from less than one part per trillion (10^{-12} mol mol^{-1} or ppt) up to a few parts per million (10^{-6} mol mol^{-1} or ppm) in the atmosphere (Wine and Nicovich, 2012). Measuring their concentration and dynamic variability in different atmospheric environments is key to addressing specific questions regarding air quality; the oxidative state of the atmosphere; the ozone budget; aerosol nucleation; and carbon, nitrogen and sulfur cycles. The understanding of the complex interactions involving those species has led to numerous investigations during the past decades.

Especially, nitrogen oxides (NO_x=NO and NO_2) have a direct impact on air quality and climate change. In the presence of volatile organic compounds (VOCs) and under solar radiation, nitrogen oxides stimulate ozone (O_3) formation in the troposphere. NO_x also plays an important role in rain acidification and ecosystem eutrophication by its transformation in nitric acid (HNO_3) (Jaworski et al., 1997; Vitousek et al., 1997). Finally, NO_x contributes to the formation of particulate matter in ambient air and to the aerosol formation leading to cloud formation (Atkinson, 2000). The NO_2 mixing ratio in the troposphere ranges from a few tens of ppt in remote areas to hundreds of parts per billion (10^{-9} mol mol^{-1} or ppb) in urban atmospheres (Finlayson-Pitts and Pitts, 2000). Being able to measure such species in situ, at low levels and at a timescale compatible with its reactivity (i.e. in min) is challenging and puts stringent constraints on the instrument sensitivity, time response, energy consumption and compactness. Among the various techniques that have so far been developed, chemiluminescence detection (CLD) (Maeda et al., 1980; Ryerson et al., 2000), long-path differential optical absorption spectroscopy (LP-DOAS) (Lee et al., 2005, 2008; Pikelnaya et al., 2007) and multi-axis differential optical absorption spectroscopy (MAX-DOAS) (Platt and Perner, 1980; Sinreich et al., 2007; Wagner et al., 2010) have been used to detect nitrogen species and halogen oxides. The CLD technique, using the chemiluminescence reaction occurring between O_3 and NO after the reduction of NO_2 into NO, is widely used for air quality measurements with sensitivities better than 100 ppt (Ryerson et al., 2000). Nevertheless, the interferences in the reduction of NO_2 to NO with other species (i.e. HONO and HNO_3) and the sensitivity to environmental conditions (temperature and humidity) leave uncertainties about absolute mixing ratio measurements (Grosjean and Harrison, 1985; Williams et al., 1998). The MAX-DOAS technique has been used to measure BrO and NO_2 by making use of the characteristic absorption features of gas molecules along a path in the open atmosphere (Leser et al., 2003). Although MAX-DOAS is relatively simple to deploy, the data analysis makes it a complex approach for in situ field measurements due to the influence of clouds on the radiative transfer which alters the path length of light (Wittrock et al., 2004; Rozanov and Rozanov, 2010). While in LP-DOAS the optical path length is known, the signal degradation due to the environment (clouds, rain and wind) remains of importance for the data retrieval, and results are integrated over the long path leading to a limited spatial resolution (Chan et al., 2012; Pöhler et al., 2010). Compact, highly sensitive and point-source measurements may be achieved using cavity enhanced techniques such as cavity ring-down spectroscopy (CRDS) and cavity-enhanced absorption spectroscopy (CEAS) (Atkinson, 2003). The potential of the CRDS for accurate, sensitive and rapid measurements in a compact and transportable instrument has already been demonstrated (Fuchs et al., 2009; Brown et al., 2002); e.g. Fuchs et al. (2009) reached a sensitivity of 22 ppt for NO_2 within 1 s of integration time using the CRDS technique. Incoherent broadband cavity-enhanced absorption spectroscopy (IBBCEAS) (Fiedler et al., 2003) is a simple and robust technique for in situ field observations. Different sources and wavelength regions have been used for the detection of NO_2 leading to different levels of performance: Venables et al. (2006) were able to detect simultaneously NO_3, NO_2, O_3 and H_2O in an atmospheric simulation chamber with a sensitivity of tens of ppb for NO_2; Gherman et al. (2008) reached ~ 0.13 and ~ 0.38 ppb for HONO and NO_2 in a 4 m^3 atmospheric simulation chamber between 360 and 380 nm; Triki et al. (2008) used a red LED source centred at 643 nm reaching a sensitivity of 5 ppb; Langridge et al. (2006) developed an instrument with a blue-light-emitting diode (LED) centred at 445 nm allowing for detection limits ranging from 0.1 to 0.4 ppb; Ventrillard-Courtillot et al. (2010) reached 600 ppt detection limit for NO_2 with an LED centred at 625 nm; and Thalman and Volkamer (2010) reported a detection limit of 30 ppt within 1 min of integration time. More recently, Min et al. (2016) proved a precision of 80 ppt in 5 s of integration at 455 nm using a spectrometer with a thermoelectric-cooled charge-coupled device (CCD) camera and very high-reflectivity mirrors. This non-exhaustive list of works underline the need of robust, compact and transportable instruments also allowing for direct multi-species detection and low detection limits for applications in remote areas such as Antarctica, where the expected mixing ratio of NO_2 could be as low as a few tens of ppt. Fuchs et al. (2010), during the NO_3Comp campaign at the SAPHIR (Simulation of Atmospheric PHotochemistry In a Large Reaction Chamber) atmospheric simulation chamber, demonstrated the potential of these optical techniques to compete with the CLD instruments as routine measurements of NO_2 concentrations in the future. The present paper describes a compact and affordable instrument based on the IBBCEAS technique, allowing for the simultaneous detection of nitrogen dioxide, iodine oxide, glyoxal and ozone (NO_2, IO, CHOCHO and O_3), with detection limits of 11, 0.3, 10 ppt and 47 ppb (1σ), respectively, for a measurement time of 22 min (half of the time is spent on the acquisition of the reference spectrum in the absence of the absorber, and the other half is spent on the absorption spectrum). The four species are directly detected by a broadband blue-light-emitting diode centred at 445 nm. The wavelength region was selected in order to optimize the detection of NO_2. Direct detection of NO is only possible in the ultraviolet region for wavelengths around 226 nm (Dooly et al., 2008) or in the mid-infrared region at 5.3 µm (Richard et al., 2018), wavelengths difficult to achieve with LED technology. Here, an indirect measurement is proposed which relies on the oxidation of NO to NO_2 under a controlled excess of O_3. The sum of NO and NO_2 is therefore measured leading to a supplemental indirect measurement of NO if the concentration of NO_2 is also monitored. The field deployment for the measurements of NO_2 and NO_x consists of two twin instruments,

IBBCEAS-NO_2 and IBBCEAS-NO_x, the later equipped with an ozone generator system.

2 Method

In IBBCEAS a broadband incoherent light source is coupled to a high-finesse optical cavity for trace gas detection. A picture of the spectrometer and a schematic diagram of the setup is shown in Fig. 1. In the present study, the broadband light source consisted of a high-power LED Luminus SBT70 allowing ~ 1 W of optical power to be injected into the resonator. A thermoelectric (TEC) Peltier cooler (ET-161-12-08-E) and a fan–heat-sink assembly were used to directly evacuate outside of the instrument up to ~ 75 W of thermal heat from the LED. A temperature regulator (RKC RF100) with a PT100 thermistor was used to stabilize the LED temperature at ± 0.1 °C. The LED spectrum was centred at 445 nm with 19 nm FWHM (full width at half maximum), which covers the main absorption features of NO_2, IO, CHOCHO and O_3. For better collimation of the LED spatially divergent emission (7 mm^2 surface), a dedicated optic (LEDiL HEIDI RS) was used and coupled with a 25 mm focal lens (L1; Thorlabs LA1951-A). The high-finesse optical cavity was formed by two 0.5 in. diameter high-reflectivity mirrors (maximum reflectivity at 450 nm $\geqslant 99.990 \pm 0.005$ %; LAYERTEC 109281) separated by a 41.7 cm long PFA (perfluoroalkoxy alkane) tube (14 mm internal diameter, 1 mm thick) held by an external stainless-steel tube. Both mirrors were pre-aligned and glued with Torr Seal epoxy glue on removable stainless-steel supports, which were then screwed on the cavity holders. This enables the easy cleaning of the mirrors when required and also the removal of the cavity tube to perform open-cavity measurements, which is of interest for the detection of the highly reactive IO radical. Behind the cavity, a Thorlabs FB450-40 filter was used in order to remove the broadband component of the radiation sitting outside the highly reflective curve of the cavity mirrors. The radiation is focused on an optical fibre (FCRL-7UV100-2-SMA-FC) using a 40 mm focal lens (L2; Thorlabs LA1422-A). The optical fibre input was composed of 7 cores in a round shape pattern on the collecting side, whereas, at the fibre end, on the spectrometer side, the cores were assembled in a line for better matching the 100 µm slit at the spectrometer. The spectrometer (Avantes AvaSpec-ULS2048L) was composed of a diffraction grating (2400 lines mm^{-1}) and 2048-pixel charge-coupled device (CCD). The resolution of the spectrometer was 0.54 ± 0.10 nm. All the optics including the cavity were mounted on a Z-shaped 8 mm thick aluminium board fixed on the rack using cylindrical dampers (Paulstra). On the board, four 5 W heating bands and one PT100 sensor were glued, and a second RKC module was used to regulate its temperature. The board therefore acts as a large radiator inside the instrument, allowing for the minimization of internal thermal gradients and thermalization of the instrument. Air circulation from outside is ensured by an aperture at the front and a fan placed at the back wall of the instrument (Fig. 1). The gas line system was composed of a manual PFA needle valve MV and a three-way two-position PTFE (polytetrafluoroethylene) valve V (NResearch 360T032) at the entrance, while a proportional valve PV (Burkert 239083), a flowmeter F (Honeywell HAFUHT0010L4AXT), a pressure sensor P (STS ATM.ECO; accuracy ± 0.2 %) and a diaphragm pump (KNF N 816 AV.12DC-B) were placed after the cavity. The entire line was made of 0.25 in. PFA tubing, which was found to be least lossy for the transport of highly reactive species (Grilli et al., 2012). The pump provided a constant flow that can reach 11 L min^{-1} at the end of the gas line, while a constant pressure in the cavity was obtained by a PID (proportional–integral–derivative) regulator on the proportional valve. A data acquisition card (National Instruments USB 6000) was interfaced to read the analogue signal from the pressure sensor, while a microcontroller (Arduino Due) derived the proportional valve. The manual valve at the entrance allowed for tuning the flow rate. At the inlet, a three-way two-position PTFE valve allowed to switch between the gas sample and zero-air mixture for acquiring a reference spectra in the absence of absorption. Zero air was produced by flowing outdoor air through a filtering system (TEKRAN 90-25360-00 Analyzer Zero Air Filter). Particle filters (Whatman® PTFE membrane filters – TE 38, 5 µm, 47 mm) were also placed in the inlet lines (reference and sample) for preventing optical signal degradation due to Mie scattering as well as a degradation of the mirror reflectivity for long-term deployment. The air flow was introduced at the centre of the cavity and extracted at both ends of the cavity. The optimal cavity design was selected by running SolidWorks flow simulations at flow rates between 0.5 and 1 L min^{-1}. Cavity mirrors were positioned in order to maximize the sample length d and to avoid localized turbulences in front of the mirrors (see Sect. S1.1 in the Supplement). The LED's power is monitored over time using a photodiode PD (Hamamatsu, S1223-01), allowing for discrimination if a decreasing of intensity at the CCD (during the acquisition of the spectra in the absence of the absorber) is due to a decreasing of the LED intensity or to the mirrors' cleanliness degradation (for more details see Sect. S1.2). All the components fit in a 19 in., 3U (5.25 in.) aluminium rack-mount case; have a total weight of 15 kg; and have a total electrical power consumption of < 300 W. The instrument interface, measurements and data analysis are performed automatically, without the intervention of an operator, by dedicated LabVIEW software. Instrument calibrations, however, must be performed by an operator on a regular basis.

3 Spectral fit

The absorption spectrum is calculated as the ratio between the spectrum of the light transmitted through the cavity with-

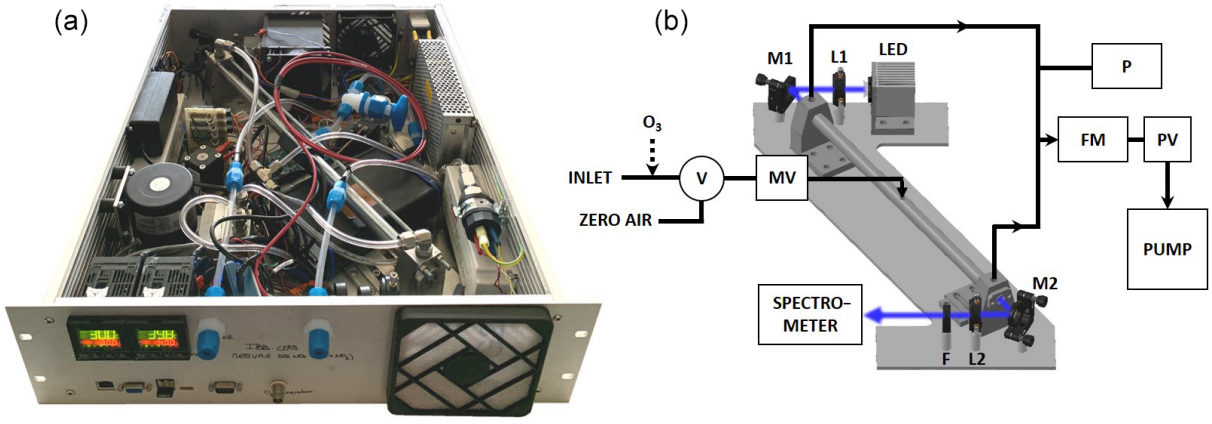

Figure 1. (a) A picture of the instrument mounted on a 19 in., 3U rack-mount case. **(b)** Schematic of the instrument. The LED is protected by a cap in which a photodiode (PD) is monitoring its power. The light from the LED is collimated by lens L1 and injected into the cavity. The exiting light is then collimated with lens L2 and injected into the spectrometer. M1 and M2 are steering mirrors, and F is an optical filter. The gas line is composed of a pump, a pressure sensor P, a flowmeter FM and a proportional valve PV. At the inlet, a three-way two-position valve in PTFE, V, is used to switch between the sample and zero air. A manual PFA needle valve MV is used to fix the flow rate. An ozonizer can be inserted in the inlet line for NO_x measurements.

out a sample, $I_0(\lambda)$, and with a sample in the cavity, $I(\lambda)$. It is expressed as the absorption coefficient (in units of cm^{-1}) by the following equation (Fiedler et al., 2003):

$$\alpha(\lambda) = \left(\frac{I_0(\lambda)}{I(\lambda)} - 1\right)\left(\frac{1 - R(\lambda)}{d}\right), \quad (1)$$

where $R(\lambda)$ is the wavelength-dependent mirror reflectivity and d the length of the sample inside the cavity. Equation (1) is derived from the Beer–Lambert law and applied to light in an optical resonator (Ruth et al., 2014). The light transmitted through the optical cavity is attenuated by different processes such as absorption, reflection and scattering of the mirror substrates and coating, as well as losses due to the medium inside the cavity. The losses of the cavity mirrors are assumed to be constant between the acquisition of the reference and the sample spectrum. Mie scattering is minimized with a 5 µm particle filter in the gas inlet, while Rayleigh scattering losses were calculated to be $2.55 \times 10^{-7}\ cm^{-1}$ at 445 nm at 25 °C and 1 atm (Kovalev and Eichinger, 2004) and thus negligible with respect to the cavity losses normalized by the cavity length $\left(\frac{1-R}{d} = 2.28 \times 10^{-6}\ cm^{-1}\right)$. Therefore, the light transmitted through the cavity is mainly affected by the absorption of the gas species, which leads to well-defined absorption spectral features, $\alpha_i(\lambda)$, that are analysed in real time by a linear multicomponent fit routine. Experimental absorption spectra of the species i ($i = NO_2$, IO, CHOCHO and O_3) have been compared with literature cross-section data accounted for the gas concentration and experimental conditions of temperature and pressure and convoluted with the spectrometer instrumental function. Those experimental spectra are then used as reference spectra for the fit.

$$\alpha(\lambda) = \sum_i \sigma_i(\lambda) c_i + p(\lambda) \quad (2)$$

A fourth order polynomial function, $p(\lambda) = a_0 + a_1\lambda + a_2\lambda^2 + a_3\lambda^3 + a_4\lambda^4$, is added to the absorption coefficient Eq. (2) to adjust the spectral baseline and account for small changes between the reference and the sample spectra. The transmitted-light intensity, as well as the optical absorption path, will be modulated by the shape of the mirror reflectivity curve. Therefore, the later should be defined in order to retrieve the correct absorption spectrum recorded at the cavity output.

4 Calibration, performance and multi-species detection

4.1 Calibration

Washenfelder et al. (2008) described a procedure for retrieving the mirror reflectivity curve by taking advantage of a different Rayleigh scattering contribution to the cavity losses while the measuring cell was filled with different bulk gases (e.g. helium versus air or nitrogen). The Rayleigh's empirical cross sections used by Min et al. (2016) and the theoretical ones used by Thalman and Volkamer (2010) were found to disagree, leading this work to propose an easier approach consisting of using trace gases at known concentrations (in this case NO_2 produced by the calibrator FlexStream™ Gas Standards Generator from KIN-TEK Analytical, Inc. and CHOCHO produced by evaporating a glyoxal solution 40 % in water from Sigma-Aldrich, since the O_3 spectrum is less structured and IO is highly reactive) and their literature cross sections (Vandaele et al., 1998, for NO_2 and Volkamer et al., 2005, for CHOCHO) for retrieving the wavelength-dependent reflectivity curve. Such an approach to calculate mirror reflectivity has been proposed before (Venables et al., 2006) and has been used by previous studies (Duan et al., 2018). The shape of the reflectivity curve

is adjusted to best match the convoluted literature NO_2 spectrum at the concentration given by the KIN-TEK calibrator (for more information, see Sect. S2). Figure 2a shows the resulting reflectivity curve and the transmitted light through the cavity and the optical filter. The maximum reflectivity achieved with both mirrors given by the calibration procedure is 99.9905 %, leading to an effective optical path length of ~ 4.4 km and a cavity finesse $\left(F = \frac{\pi\sqrt{R}}{(1-R)}\right)$ of $\sim 33\,100$. While the shape of the mirror reflectivity curve is determined once and for all, its offset is slightly adjusted after each mirrors' cleaning, by flushing in the cavity a known concentration of NO_2. The spectral emission of the LED centred at 445 nm is well suited also for the detection of IO, CHOCHO and O_3, which are other key species in atmospheric chemistry. For the field measurements of NO_2 and NO_x, two twin instruments named IBBCEAS-NO_2 and IBBCEAS-NO_x are deployed, with the later equipped with an ozone generator on the gas inlet line. At this wavelength region, water vapour also absorbs and is accounted for in the spectral-fit analysis. However, the absorption of oxygen dimer is not required in the fit routine, since the absorption feature will be present in the reference (I_0) as well as in the absorption (I) spectra. In Fig. 2b simultaneous detection of NO_2, IO and O_3 is reported. Ozone, at 28.9 ppm, is produced by water electrolysis as described in Sect. 4.4; 191.8 ppb of NO_2 is provided by a permeation tube, and 425.6 ppt of IO is generated by photochemical reaction of sublimated iodine crystals and ozone in the presence of radiation inside the cavity. For this spectrum, the light transmitted is integrated for 350 ms on the CCD and averaged over 1000 spectra, yielding to a 1σ standard deviation of the residuals of 4×10^{-8} cm^{-1} (Fig. 2b bottom). In Fig. 2c simultaneous detection of NO_2, CHOCHO and H_2O is reported. CHOCHO at 4.3 ppb is produced by evaporating a glyoxal solution (40 % in water; Sigma-Aldrich) at the sample gas inlet of the instrument; NO_2 at 1.40 ppb and H_2O at 0.54 % are ambient concentrations observed in the laboratory during the experiment. For this spectrum, the light transmitted is integrated for 250 ms on the CCD and averaged over 1000 spectra, yielding to a 1σ standard deviation of the residuals of 5×10^{-9} cm^{-1} (Fig. 2c bottom). The top of Fig. 2b and c shows the experimental spectra (black traces), the fit result (red traces) and contributions from each species (middle) which are included in the spectral fit. The concentrations of the species are retrieved with respect to the literature cross sections using the calibrated reflectivity curve discussed above.

4.2 Instrumental calibration and intercomparison

A calibrator (FlexStream™ Gas Standards Generator, KIN-TEK Analytical, Inc.) was used to produce a stable NO_2 source. The sample was produced using a permeation tube of NO_2 (KIN-TEK ELSRT2W) calibrated at an emission rate of 115 ng min^{-1} at 40 °C loaded into the calibrator. This type of calibrator is ideally suited for creating trace concentration mixtures (from ppt to ppm). The instruments were calibrated against the calibrator delivering NO_2 at 49.59 ± 0.17 ppb. To confirm the calibration process as well as the stability of the instrument within a greater range of concentrations, two intercomparisons of the IBBCEAS with two different CLD instruments (Thermo Fisher™ 42i NO_x analyser and Thermo Fisher™ 42iTL NO_x trace analyser) were performed in outdoor air over 39 and 12 h, respectively. Results are reported in Fig. 3. The experiments took place at the Institute of Environmental Geosciences (IGE) in Saint-Martin-d'Hères, France. The IGE is located in the university campus, ~ 1 km from the city centre of Grenoble and ~ 300 m from a highway. Ambient air was pumped simultaneously from the same gas line by the instruments at flow rates of 1.0 and 0.5 L min^{-1} for the IBBCEAS and the CLD instrument (Thermo Fisher™ 42i NO_x analyser), respectively. The measurements were conducted in September 2018. On the evening of Saturday, 29 September, the NO_2 peak occurred at a slightly later time than normally expected (from 20:00 to midnight; Fig. 3a). This may be due to the fact that on a Saturday night, urban traffic can be significant until late, but it also may be due to severe weather conditions prevailing at this time, with a storm and lightning known to be a major natural source of NO_x (Atkinson, 2000). For the second experiment shown in Fig. 3b, ambient air was pumped at flow rates of 1.0 and 0.8 L min^{-1} for the IBBCEAS and the CLD trace instrument (Thermo Fisher™ 42iTL NO_x trace analyser), respectively. The measurements were conducted in July 2019. Both instruments showed the expected variability of an urban environment with an increase of NO_2 in the evening and morning due to photochemical processes and anthropogenic activities (i.e mainly urban traffic).

The correlation plot, based on data of all instruments, in Fig. 4a, shows good linearity with a slope of 1.088 ± 0.005 and a correlation coefficient of $R^2 = 0.989$ with measurements averaged over 5 min. In order to perform linearity tests, the previous NO_2 FlexStream™ calibrator was used to produced various concentrations of NO_2 covering a large range of concentrations. Figure 4b shows the good linearity, from the ppt to ppb range, of the IBBCEAS instrument with a slope of 1.015 ± 0.006 and a correlation factor of $R^2 = 0.9996$, confirming the validity of the calibration approach. The discrepancies observed between the IBBCEAS and the CLD techniques might be explained by positive and negative interferences on the CLD technique. While the system presented here measures NO_2 directly, the CLD technique applies an indirect measurement of NO_x from the oxidation of NO through a catalyser, then in CLD; the NO_2 mixing ratio is obtained by the subtraction of the NO signal to the total NO_x signal. Villena et al. (2012) demonstrate that the interferences on an urban atmosphere for the CLD technique implied positive interferences when NO_y species photolysis occurred, leading to an overestimation of daytime NO_2 levels, while negative interferences were attributed to

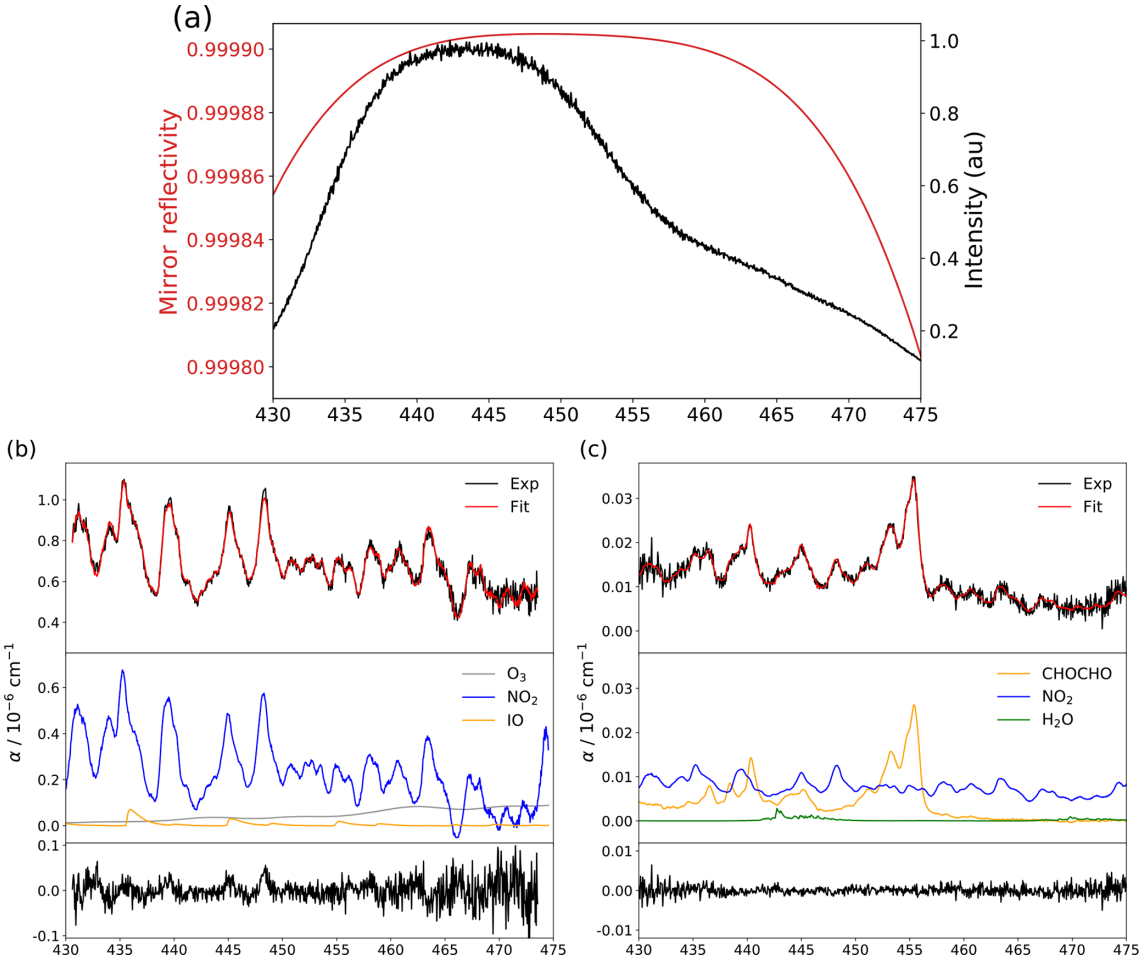

Figure 2. **(a)** The mirror reflectivity curve (red) in comparison with the spectrum of the LED light transmitted by the cavity and the optical filter for a single acquisition of 250 ms. **(b)** In black, an example of an experimental spectrum of NO_2, IO and O_3 at concentrations of 191.8 ppb, 425.6 ppt and 28.9 ppm, respectively; in red, the multi-species spectral fit; and in blue, orange and grey the absorptions of the different species. At the bottom (in black) the residual of the experimental fit with a 1σ standard deviation of 4×10^{-8} cm^{-1} after 1000 averages. **(c)** In black, an example of an experimental spectrum of NO_2, CHOCHO and H_2O at concentrations of 1.40 ppb, 4.3 ppb and 0.54 %, respectively; in red, the multi-species spectral fit; and in blue, orange and green the absorptions of the different species. At the bottom (in black) the residual of the experimental fit with a 1σ standard deviation of 5×10^{-9} cm^{-1} after 1000 averages.

the VOCs photolysis followed by peroxy radical reactions with NO.

4.3 Instrument sensitivity and long-term stability

In remote areas such as East Antarctica, NO_2 ranges from a few tens to a few hundreds of ppt (50–300 ppt) (Frey et al., 2013, 2015). Due to the low signal-to-noise ratio of the spectrometer, a single acquired spectrum (with an integration time ranging between 200 and 350 ms) does not provide the required detection limit. However, the sensitivity can be improved by averaging the measurements for longer times, over which the instrument is stable. The stability of the IBBCEAS system is mainly affected by temperature fluctuations, mechanical instabilities and pressure drifts. In order to characterize the long-term stability of the instrument, two different studies were conducted on the IBBCEAS-NO_2 during the Antarctica field campaign at Dome C in 2019–2020 (the same results for the IBBCEAS-NO_x can be found in the Supplement). For both studies, the light transmitted through the cavity (I) was integrated at the CCD for 250 ms, providing a signal-to-noise ratio of 110 for a single spectrum. The reference spectrum (I_0) was taken by averaging 2000 individual spectra ($\sim$ 8 min) while flushing the cavity with zero air. Subsequently, a 9 h long time series was recorded for each instrument maintaining the zero-air flow. The instrument was regulated at 12.0 ± 0.2 °C, with a cavity pressure of 630.0 ± 0.7 mbar and a gas flow of 1.02 ± 0.11 L min^{-1}. The minimum absorption coefficient ($\alpha_{\min}$), corresponding to the standard deviation of the residual of the spectrum, was deduced for different time aver-

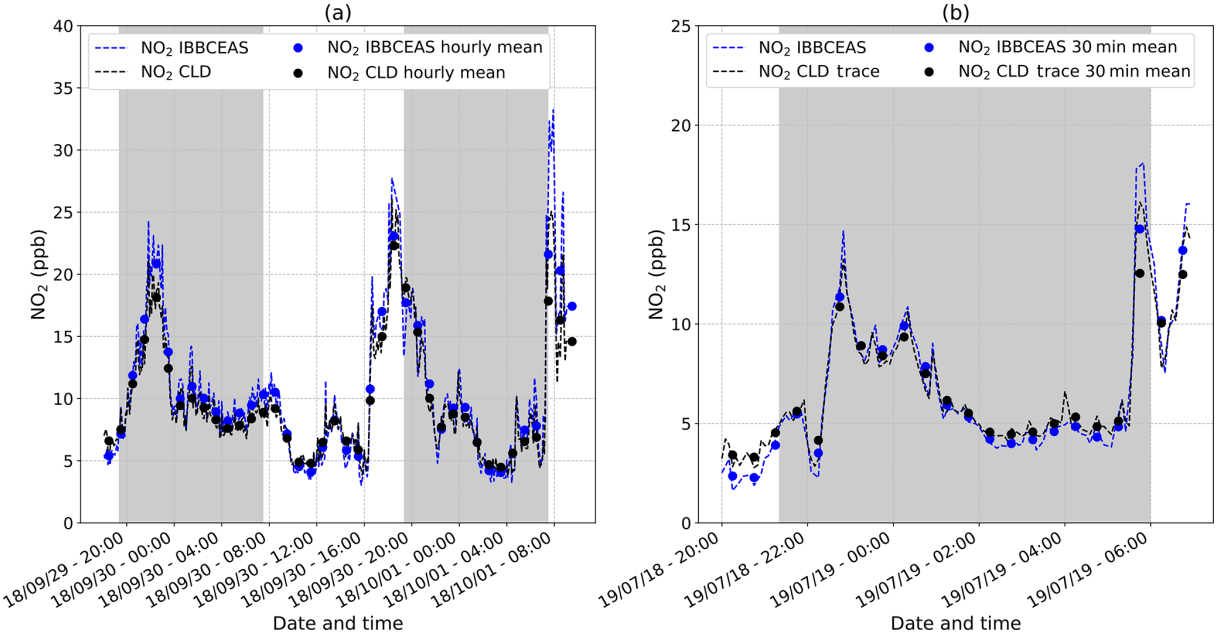

Figure 3. (a) A 39 h long intercomparison of the IBBCEAS instrument and the commercial CLD instrument (Thermo Fisher™ 42i analyser) on the NO_2 detection in an outdoor urban area performed in September 2018 (dates in the format of two-digit year/month/day). The plot reports continuous (dashed lines) and hourly (dots) average data for both techniques. The grey area corresponds to the nighttime period. **(b)** A 12 h long intercomparison of the IBBCEAS instrument and the commercial CLD trace instrument (Thermo Fisher™ 42iTL trace analyser) on the NO_2 detection in an outdoor urban area performed in July 2019. The plot reports continuous (dashed lines) and 30 min (dots) average data for both techniques. The grey area corresponds to the nighttime period.

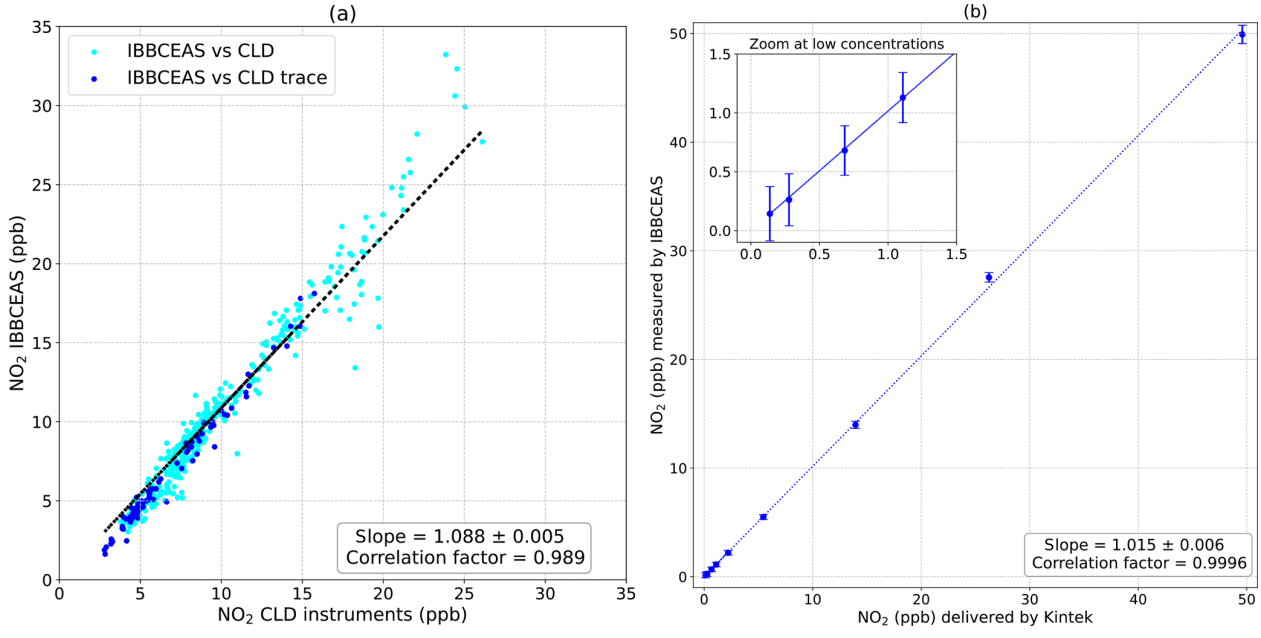

Figure 4. (a) A linear correlation was obtained with a slope of 1.088 ± 0.005 and a correlation coefficient of $R^2 = 0.989$ between the IBBCEAS system and the Thermo Fisher instruments. **(b)** Results of the system's calibration using an NO_2 FlexStream™ calibrator. A linear correlation was obtained with a slope of 1.015 ± 0.005 and a correlation coefficient of $R^2 = 0.9996$.

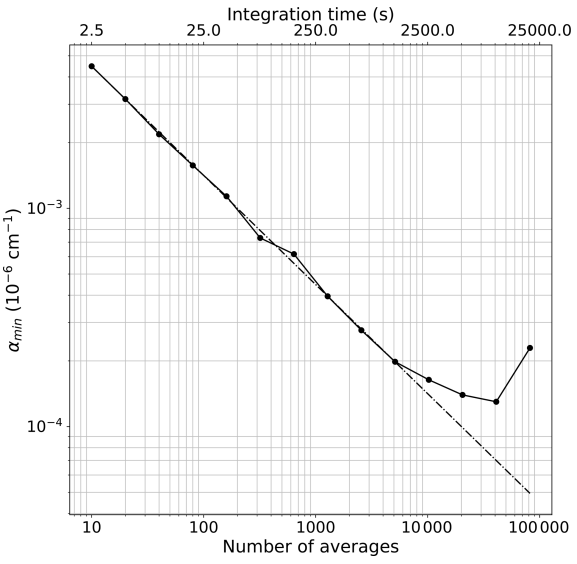

Figure 5. The minimum absorption coefficient $\alpha_{\min}$ versus the number of spectral average for the IBBCEAS-NO_2 instrument. For these measurements the cell was continuously flushed with a flow of 1.02 L min^{-1} of zero air, and the $\alpha_{\min}$ was calculated from the standard deviation of the residual of the spectra at different time averages.

ages. The results are shown in the log–log plot of Fig. 5, where the dots are the data and the dashed line indicates the trend in the case of a pure white-noise regime. From the graph one can see that the instrument follows the white-noise trend for about 22 min (5200 averages); afterwards, the baseline noise starts to deviate due to the rise of frequency-dependent noise. The chosen $\alpha_{\min}$ value corresponds to 2.0×10^{-10} cm^{-1} within $\sim$ 22 min (5200 spectra) of measurement during which a reference spectrum in the absence of absorbers and the absorption spectrum are acquired. The corresponding figure of merit (noise-equivalent absorption sensitivity – NEAS – or $\alpha_{\min(\mathrm{BW})} = \alpha_{\min} \times \sqrt{\frac{t_{\mathrm{int}}}{M}}$) is therefore 1.8×10^{-10} cm^{-1} Hz$^{-1/2}$ per spectral element (with t_{int} being the integration time of $\sim$ 11 min and M being the number of independent spectral elements; here 800 spectral elements are considered for the spectral fit).

For the same time series, an Allan–Werle (AW) statistical method on the measured concentrations was employed (Werle et al., 1993). In this case, spectra were averaged in a block of 10 and analysed by the fit routine. The results of the fit are reported (Fig. 6a). For an acquisition time of 2.5 s, corresponding to 10 averaged spectra, the AW standard deviation $\sigma_{\text{AW-SD}}$ was 175, 4.8, 125 ppt and 725 ppb for NO_2, IO, CHOCHO and O_3, respectively. By increasing the integration time, the $\sigma_{\text{AW-SD}}$ decreased following the white-noise trend, the coloured dashed line of Fig. 6b, with a characteristic $\sqrt{N}$ slope (where N is the number of averaged spectra). Because a reference spectrum in the absence of absorbers is required by this CEAS technique, depending on the shape of the AW plot, different strategies may be followed. In our case, the AW trends continue to decrease for all species for $\sim$ 22 min (5200 averages); this means that one can spend 11 min acquiring the reference spectrum and a further 11 min for the absorption spectrum, leading to limits of detection (LODs) of 11, 0.3, 10 ppt and 47 ppb (1σ) for NO_2, IO, CHOCHO and O_3, respectively. In our case, we chose to divide the measurement times by 2 (i.e. $\sim$ 11 min and 2600 averages for acquiring both the reference and the absorption spectra), offering equally interesting LODs: 16, 0.4, 12 ppt and 72 ppb for NO_2, IO, CHOCHO and O_3 (1σ), respectively, and allowing us to stay within the white-noise regime.

The long-term stability and repeatability of the instrument were further studied by taking regular reference spectra within the optimum integration time of the instrument while continuously flushing the instrument with the zero-air mixture. In this case $\sim$ 5 and $\sim$ 3 min intervals were chosen, corresponding to 1024 and 580 averages (for 350 and 300 ms integration time, respectively) and a sensitivity on the NO_2 concentrations of 55 and 53 ppt (1σ), respectively. The results are reported in Fig. 7. Test_1 (1024 averages) was run for 9h, and Test_2 (580 averages) was run for 15 h. These tests highlight the reliability of the measurement protocol, with the long-term measurement well distributed within the 3σ level of the measurements precision (165 and 159 ppt, respectively). A boxplot is also reported representing the average values (green triangles) and medians, quartiles, and minimum and maximum values. The histogram analysis of those tests show a good distribution of the measurements within the 3σ level.

Table 1 shows a comparison between the instrument presented in this work and other recently developed IBBCEAS systems. The detection limits are given in ppt min^{-1} (1σ) with the normalization time that accounts for the acquisition of the reference (without absorption) and sample spectra to allow for a better comparison. It should be noticed that all the other developments took advantage of an optical spectrometer with a cooled CCD device to reduce dark noise. A more compact and affordable spectrometer was preferred in this work. The cooling at the CCD would allow for a gain of up to a factor of 10 on the signal-to-noise ratio, which would directly apply to the achievable detection limits. Furthermore, a CCD with a higher sensitivity would allow for selecting higher-reflectivity mirrors and increase the optical pathlength. Noteworthy, the optimum integration time, corresponding to a minimum of the $\sigma_{\text{AW-SD}}$, is at 1300 s ($\sim$ 22 min), allowing for the achievement of low detection limits even without a cooled CCD.

4.4 Indirect measurement of NO

Measuring NO and NO_2 simultaneously is important to study the NO_x budget in the atmosphere. In the selected blue vis-

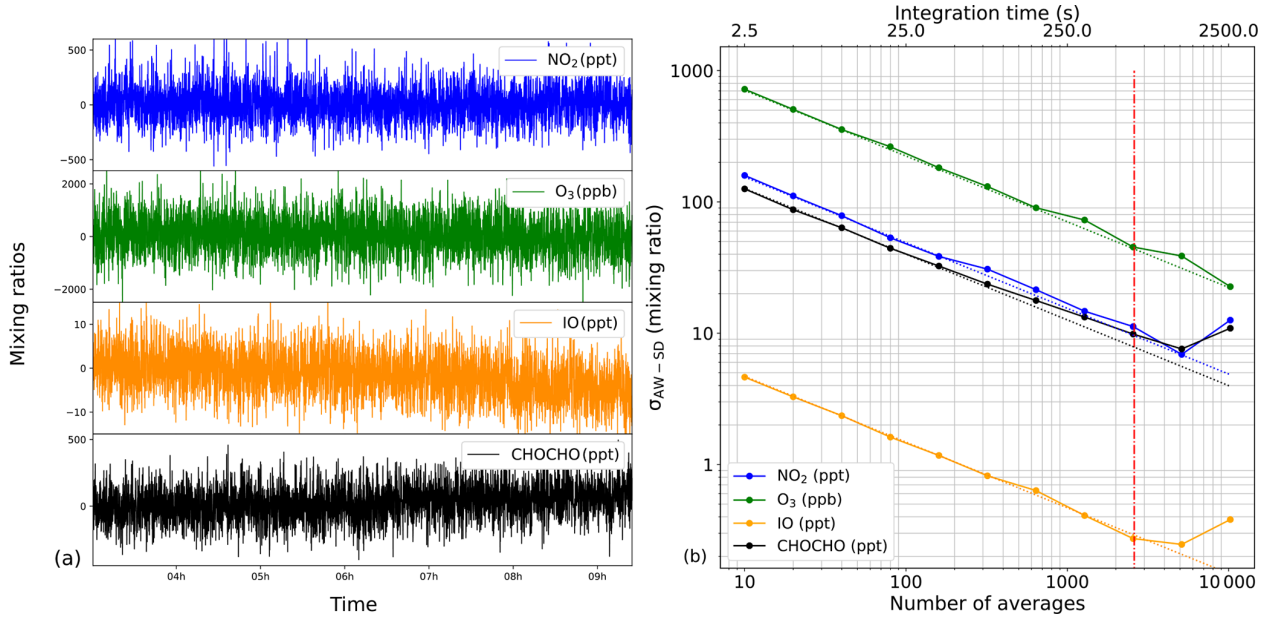

Figure 6. **(a)** Mixing ratios of the target species NO_2, O_3, IO and CHOCHO measured during a 9 h Allan–Werle variance statistical experiment flowing zero air through the cavity on the IBBCEAS-NO_2 instrument. **(b)** The log–log Allan–Werle standard deviation plot, illustrating that the instrument performance follows the white-noise regime up to a certain extent, identified by the dashed lines. This represents the optimum integration time, after which instrumental instabilities start to dominate.

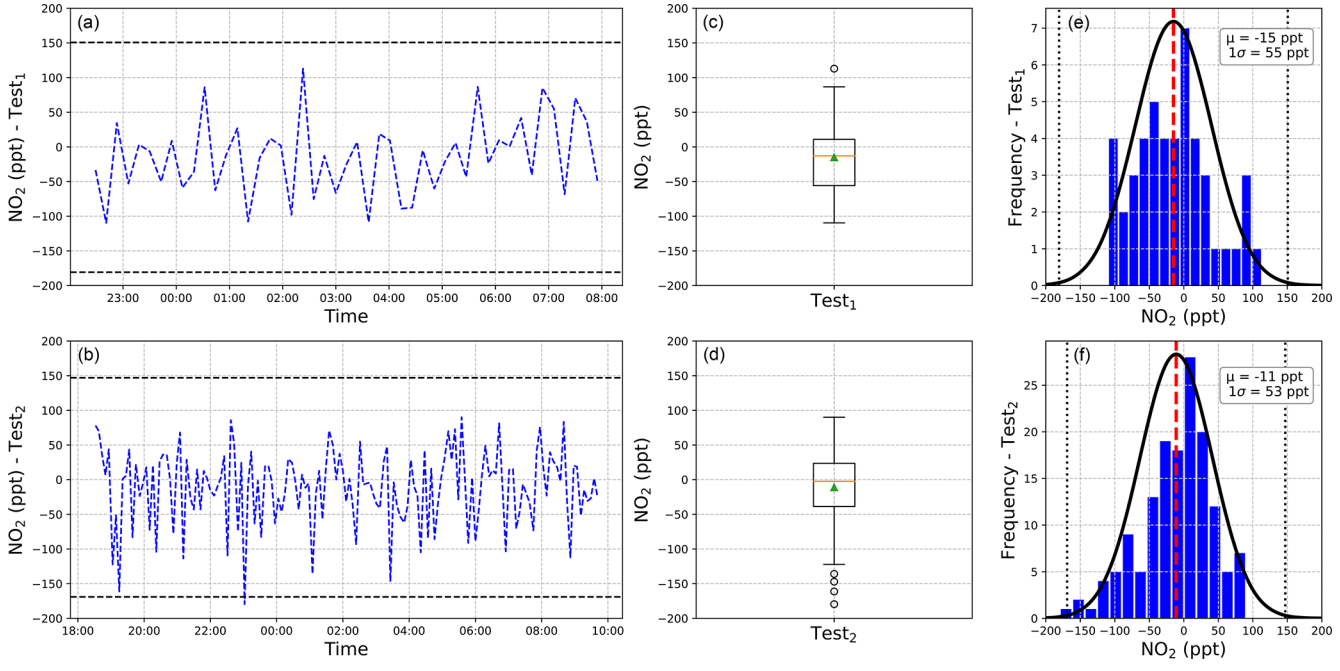

Figure 7. **(a, b)** Time series of two long-term stability tests, with the black dashed lines representing the 3σ level; **(c, d)** boxplot of the stability test while continuously flushing zero air in the cavity, with means over 46 and 148 measurements (for $Test_1$ and $Test_2$, respectively) shown as green triangles and dots representing the outliers; **(e, f)** histogram analysis showing well distributed measurements within the 3σ level (black dashed lines).

Table 1. Performance comparisons with other recently developed IBBCEAS systems.

References	Centred wavelength (nm)	Source FWHM (nm)	NO_2 detection limit (ppt min^{-1})	Sample path length (cm)	Mirror reflectivity (%)	Optical length (km)	Mirrors purged	CCD cooled (°C)	Minimum $\sigma_{AW\text{-}SD}$ deviation (s)
Min et al. (2016)	455	18	16	48	99.9973	17.8	no	−70	100
Jordan et al. (2019)	505	30	200	102	99.98	5.1	yes	−80	300
Liu et al. (2019)	455	18	33	84	99.993	10.3	yes	−70	100
Liang et al. (2019)	448	15	15	58.9	99.9942	11.7	yes	−10	3500
This work	450	19	40	41.7	99.9905	4.4	no	no	1300

ible region, there are no NO absorption features for direct optical measurements, and optical absorption detection of NO is typically done in the infrared region (Richard et al., 2018). However, its detection can be performed by indirectly measuring NO_2 after chemical conversion of NO to NO_2 in a controlled O_3 excess environment. This will lead to the measurement of NO_x, which, coupled with a simultaneous detection of NO_2 will provide the concentration of NO ($[NO]=[NO_x]-[NO_2]$) (Fuchs et al., 2009):

$$NO + O_3 \rightarrow NO_2 + O_2$$
$$k_1 = 1.80 \times 10^{-14}\,cm^3\,molec^{-1}\,s^{-1} \text{ at } 25\,°C. \quad \text{(R1)}$$

O_3 was produced by electrolysis of water using commercial ozone micro cells (INNOVATEC) allowing for the generation of O_3 without nitrogen oxide impurities and without the need of an oxygen gas bottle. The cells were mounted in a homemade plastic container offering a 200 cm^3 water reservoir. With a miniaturized design (15 cm × 15 cm × 15 cm), ozone production can be controlled upon injection into the inlet line. The sample air flow to be analysed works as carrier gas for flushing the ozone-enriched surface water. This design also prevents the production of unwanted oxidizing agents such as peroxides, as well as sample dilution, causing a signal degradation and requiring precise flow measurements for quantitative analysis. The production of O_3 is controllable by the amount of electrolytic cells used and the supplied current, offering a dynamic range of 0–50 ppm of O_3 for a 1 L min^{-1} total flow rate. A diagram and details of the system can be found in Sect. S3.2. For long-term use of the instrument, the overall water consumption should be considered. Losses due to evaporation were estimated to be between 7 and 30 $cm^3\,d^{-1}$ at 10 and 30 °C, respectively, for a flow rate of 1 L min^{-1}, while losses due to electrolysis are negligible, with only 0.024 $cm^3\,d^{-1}$ of consumption. The other parameter to consider is the mixing time between the ozone generator and the measurement cell with respect to the O_3 excess. For instance, the calculated production rate of NO_2 from Reaction (R1) (i.e. reaction speed or conversion rate of NO) is $v = 4.20 \times 10^{11}$ molec $cm^3\,s^{-1}$ for 5 ppb of NO and 8 ppm of O_3. Under these conditions, a mixing time of 0.29 s is required for completing the conversion. With an air flow of 1 L min^{-1}, a 40 cm long 4 mm internal-diameter tube is therefore required between the ozone generator and the measurement cell. The performance of the ozone generation system was tested on the IBBCEAS instrument with a nitrogen oxide standard gas bottle containing ∼ 195 ppb of NO in air (Air Liquide). Kinetic simulations using Tenua software (Wachsstock, 2007) were made in order to establish the O_3 excess concentrations needed to achieve the complete conversion of NO to NO_2, which, along with its detection, was tested with the IBBCEAS instrument by varying the excess concentration of O_3 until complete conversion of NO was achieved at different flows (i.e. different reaction times before reaching the measurement cell). The experimental results were in good agreement with the simulations as reported in Fig. S9. In addition, the instrument was found to have a linear response regarding the detection of the produced O_3. The detection limit for the NO_x measurement was found to be similar to the one of NO_2, 10 ppt (1σ) in 22 min of integration time, while for NO, retrieved as the difference between the NO_x and the NO_2 concentrations, the detection limit estimated from the error propagation corresponds to 21 ppt.

5 Possible chemical and spectral interferences

Further possible interferences on NO_2 detection in the presence of high levels of O_3 were also studied, since a large excess of O_3 could trigger the following reactions with rate constants that are a few orders of magnitude lower than k_1 (from the NIST Kinetics Database):

$$NO_2 + O_3 \rightarrow NO_3 + O_2$$
$$k_2 = 3.8 \times 10^{-17}\,cm^3\,molec^{-1}\,s^{-1} \text{ at } 25\,°C \quad \text{(R2)}$$
$$NO_2 + O_3 \rightarrow 2O_2 + NO$$
$$k_3 = 1.0 \times 10^{-18}\,cm^3\,molec^{-1}\,s^{-1} \text{ at } 25\,°C \quad \text{(R3)}$$
$$NO_3 + O_3 \rightarrow 2O_2 + NO_2$$
$$k_4 = 1.0 \times 10^{-17}\,cm^3\,molec^{-1}\,s^{-1} \text{ at } 25\,°C. \quad \text{(R4)}$$

To study those possible interferences, 100 ppb of NO_2 produced by a permeation tube were pumped through the ozonizer and the spectrometer at a flow rate of 1 L min^{-1} while varying the concentration of O_3 from 0 to 10 ppm.

The NO_2 concentration was stable at low ozone concentrations, while a drop of 14 % was observed at high levels of O_3 ($\geqslant$8 ppm). Kinetics simulations showed that the NO_2 consumption in favour of the NO_3 production ($NO_2 + O_3 \rightarrow NO_3 + O_2$) was kinetically possible under those conditions. The consumption of NO_2 is strongly dependent on the reaction time and the concentration of O_3. The later should be selected according to the reaction time imposed by the volume of the inlet line and the flow rate, therefore making this interference negligible. Other chemical reactions could led to an overestimation of NO_2 mixing ratios:

$$\mathrm{HONO} \rightarrow \mathrm{NO} + \mathrm{HO}$$
$$k_5 = 3.9 \times 10^{-21}\,\mathrm{cm^3\,molec^{-1}\,s^{-1}} \text{ at } 25\,^{\circ}\mathrm{C} \quad \text{(R5)}$$
$$\mathrm{HO_2NO_2} \rightarrow \mathrm{NO_2} + \mathrm{HO_2}$$
$$k_6 = 1.3 \times 10^{-20}\,\mathrm{cm^3\,molec^{-1}\,s^{-1}} \text{ at } 25\,^{\circ}\mathrm{C}. \quad \text{(R6)}$$

Couach et al. (2002) estimated the background levels of HONO and HO_2NO_2 in Grenoble to be 4 and 2 ppq (or 10^{-15} mol mol^{-1}; parts per quadrillion), respectively (Couach et al., 2002). With such low concentrations and kinetic constant rates, interferences due to Reactions (R5) and (R6) can be neglected in an urban environment. However, in remote areas such as the East Antarctic Plateau, HO_2NO_2 levels were estimated by indirect measurements to be around 25 ppt (Legrand et al., 2014). Because the lifetime of HO_2NO_2 decreases with temperature ($\tau_{HO_2NO_2} = 8.6$ h at $-30\,^{\circ}$C and 645 mbar), its measurement using an instrument stabilized at higher temperature would lead to an overestimation of the NO_2 due to the thermal degradation of the HO_2NO_2. However, this interference can be minimized by working at low temperatures: at 10 °C and 1 L min^{-1} flow in our IBBCEAS instrument, the NO_2 signal would be overestimated by only 1 ppt, which is below the detection limit of the sensor. The instruments were therefore designed for working at low temperatures (up to a few degrees Celsius). One more reaction, Reaction (R7), may also lead to possible interferences for NO_2 detection:

$$\mathrm{HONO} + \mathrm{OH} \rightarrow \mathrm{NO_2} + \mathrm{H_2O}$$
$$k_7 = 4.89 \times 10^{-12}\,\mathrm{cm^3\,molec^{-1}\,s^{-1}} \text{ at } 25\,^{\circ}\mathrm{C}. \quad \text{(R7)}$$

In urban environments OH radicals of up to 4×10^6 OH radicals cm^{-3} can be observed (Heard, 2004; Mauldin et al., 2001). With background levels of HONO such as 4 ppq in the city of Grenoble and around 30 ppt in Dome C, Antarctica (Legrand et al., 2014), very low mixing ratios of NO_2 (< few ppq) would be produced by Reaction (R7) in less than 8 s (residence time of the molecules in the instrument at 1 L min^{-1}). Therefore, contribution from this interference can be neglected. Previous works also highlighted possible artefacts through the heterogenous reaction of NO_2 and H_2O occurring in thin films on surfaces: the approximate rate production of HONO plus NO calculated in their study was reported to be between 4×10^{-2} and 8×10^{-2} ppb min^{-1} ppm^{-1} of NO_2 (Finlayson-Pitts et al., 2003). Assuming linearity between production rates and concentrations, this would represent a range of 8 to 16 ppq for 200 ppt of NO_2 in remote areas such as the East Antarctic Plateau. The losses that may occur on the thin films on surfaces through the heterogeneous reaction of NO_2 and H_2O are therefore negligible. Finally, detection of NO_2, CHOCHO and IO may be affected by spectral interferences. For instance, water vapour also shows an absorption signature at this wavelength region which was included in the fit routine. Its spectral fit is important particularly for the measurement of NO_x, where the inlet sampling line gets saturated in water vapour while passing through the water reservoir of the ozone generator. In addition, artefacts on the signal and the spectral fit were studied by varying the O_3, NO_2 or NO mixing ratios in the cavity. Small imperfections of the fit could lead to large effects on the NO_2 retrieved mixing ratio, particularly at sub-ppb concentrations and in the presence of large amounts of ozone. However, no appreciable effects of possible artefacts were observed while O_3 concentrations of up to 8 ppm were used. These performance studies and the simplicity of the ozone generator, compact and fully controllable, make it suitable for field applications.

6 Conclusions

A compact, robust, affordable and highly sensitive IBBCEAS instrument for direct detection of NO_2, IO, CHOCHO and O_3 and indirect detection of NO is reported in this work. The instrument relies on the injection of incoherent radiation from a compact, high-power and low-cost LED source, into a high-finesse optical cavity. The instrument provides a minimum detectable absorption of 2.0×10^{-10} cm^{-1} corresponding to a figure of merit (noise-equivalent absorption sensitivity; NEAS) of 1.8×10^{-10} cm^{-1} Hz$^{-1/2}$ per spectral element. Due to the multiplexing broadband feature of the setup, multi-species detection can be performed with simultaneous detection of NO_2, IO, CHOCHO and O_3 achieving detection limits of 11, 0.3, 10 ppt and 47 ppb (1σ) within 22 min of measurement (which account for the reference and absorption spectra acquisition), respectively. Detection limits for the indirect measurement of NO_x and NO are 10 and 21 ppt (1σ), respectively. The instrument has been designed to fit in a 19 in., 3U rack-mount case; weighs 15 kg; and has a total electrical power consumption of < 300 W. The detection limits could be further improved by replacing the Avantes ULS2048L spectrometer, which offers at this working wavelength a signal-to-noise ratio on a single acquisition of 110 and a sensitivity of 172 000 counts μW^{-1} ms^{-1}, with a spectrometer with an integrated cooled CCD. The cooling would allow to gain up to a factor of 10 on the signal-to-noise ratio, which would directly apply to the detection limits. Better sensitivity of the CCD would also allow for

the use of higher-reflectivity mirrors as done by Min et al. (2016), providing an effective optical path length of ~ 18 km (with a similar cavity length), ~ 4 times higher than the one obtained in this work. The dynamic ranges, detection limits and multi-species detection character make this instrument well suited for measurements in different environments, from highly polluted to very remote areas such as polar regions. The instruments can be used in the future to address different scientific questions, related to the oxidative capacity at particular regions (i.e. inland and coastal polar atmospheres), where variability of NO_x and IO would provide key information for understanding the mechanisms taking place in such remote areas. The detection of the α-dicarbonyl CHOCHO may have applications at the marine boundary layer, where its source remains unknown and its contribution to secondary aerosol particle formation may be relevant (Ervens et al., 2011; Volkamer et al., 2007; Fu et al., 2008).

Data availability. The data are available upon request.

Supplement. The supplement related to this article is available online at: https://doi.org/10.5194/amt-13-4317-2020-supplement.

Author contributions. Grants obtained by JS, AD and RG funded the project. The IBBCEAS instruments were designed and developed by CB under the supervision of RG. AB developed and validated the ozone generation. The instruments were optimized and validated by CB and AB, who also did the instrumental intercomparison, the measurements for the long-term stability and the simulations and study of the possible chemical interferences. RG was the principal supervisor of the project. JS and AD contributed with their knowledge in atmospheric sciences, and they closely followed the project with regular meetings. JS and RG are the supervisors of AB's PhD thesis under which the instruments are deployed. NC provided technical and engineering input particularly at the beginning of the project. The paper was written by AB, CB and RG, with contributions from all authors .

Competing interests. The authors declare that they have no conflict of interest.

Acknowledgements. The authors would like to thank the Labex OSUG@2020 for funding the Thermo Fisher™ 42i NO_x analyser and IPEV for funding the Thermo Fisher 42iTL™ NO_x trace analyser that were used during the development of the IBBCEAS instruments presented here. The authors thank Guillaume Méjean and Daniele Romanini from LiPhy, France, for the very useful exchange of information regarding IBBCEAS techniques as well as Andy Albert Ruth from the University of Cork, Ireland, for his very useful feedback on the paper. The authors thank Stephan Houdier for discussions about glyoxal measurement. And finally, the authors greatly thank the technical staff of the IGE for their technical support.

Financial support. The research leading to these results has received funding from the PARCS project (Pollution in the Arctic System, a project of the CNRS French Arctic Initiative at https://parcs.aeris-data.fr/, last access: 27 March 2020), the Labex OSUG@2020 ("Investissements d'avenir" ANR10 LABX56), the French national programme LEFE (Les Enveloppes Fluides et l'Environnement), the Agence Nationale de la Recherche (ANR; contract no. ANR-16-CE01-0011-01 EAIIST), the BNP Paribas Foundation through its Climate & Biodiversity Initiative, and the French Polar Institute (IPEV) through programmes 1177 (CAPOXI 35–75) and 1169 (EAIIST).

Review statement. This paper was edited by Hendrik Fuchs and reviewed by two anonymous referees.

References

Atkinson, D. B.: Solving chemical problems of environmental importance using Cavity Ring-Down Spectroscopy, Analyst, 128, 117–125, https://doi.org/10.1039/b206699h, 2003.

Atkinson, R.: Atmospheric chemistry of VOCs and NOV, Atmos. Environ., 34, 2063–2101, https://doi.org/10.1016/S1352-2310(99)00460-4, 2000.

Brown, S. S., Stark, H., Ciciora, S. J., McLaughlin, R. J., and Ravishankara, A. R.: Simultaneous in situ detection of atmospheric NO_3 and N_2O_5 via Cavity Ring-Down Spectroscopy, Rev. Sci. Instrum., 73, 3291–3301, https://doi.org/10.1063/1.1499214, 2002.

Chan, K. L., Pöhler, D., Kuhlmann, G., Hartl, A., Platt, U., and Wenig, M. O.: NO_2 measurements in Hong Kong using LED based long path differential optical absorption spectroscopy, Atmos. Meas. Tech., 5, 901–912, https://doi.org/10.5194/amt-5-901-2012, 2012.

Couach, O., Balln, J., Jimenez, R., Rjstorj, P., Simeonov, V., Quaglla, P., and Clappier, A.: Etude d'un épisode photochimique à l'alde d'un modèle méso-échelle et de mesures intensives sur la région de Grenoble – Study of a photochemical episode over the Grenoble area using a mesoscale model and intensive measurements, Pollution atmosphérique, 174, 277–295, 2002.

Dooly, G., Fitzpatrick, C., and Lewis, E.: Deep UV based DOAS system for the monitoring of nitric oxide using ratiometric separation techniques, Sensor. Actuat. B Chem., 134, 317–323, https://doi.org/10.1016/j.snb.2008.05.011, 2008.

Duan, J., Qin, M., Ouyang, B., Fang, W., Li, X., Lu, K., Tang, K., Liang, S., Meng, F., Hu, Z., Xie, P., Liu, W., and Häsler, R.: Development of an incoherent broadband cavity-enhanced absorption spectrometer for in situ measurements of HONO and NO_2, Atmos. Meas. Tech., 11, 4531–4543, https://doi.org/10.5194/amt-11-4531-2018, 2018.

Ervens, B., Turpin, B. J., and Weber, R. J.: Secondary organic aerosol formation in cloud droplets and aqueous particles (aqSOA): a review of laboratory, field and model studies, Atmos.

Chem. Phys., 11, 11069–11102, https://doi.org/10.5194/acp-11-11069-2011, 2011.

Fiedler, S. E., Hese, A., and Ruth, A. A.: Incoherent Broad-Band Cavity-Enhanced Absorption Spectroscopy, Chem. Phys. Lett., 371, 284–294, https://doi.org/10.1016/S0009-2614(03)00263-X, 2003.

Finlayson-Pitts, B. J. and Pitts, J. N.: Chapter 4 – Photochemistry of important atmospheric species, in: Chemistry of the Upper and Lower Atmosphere, edited by: Finlayson-Pitts, B. J. and Pitts, J. N., Academic Press, San Diego, USA, 86–129, https://doi.org/10.1016/B978-012257060-5/50006-X, 2000.

Finlayson-Pitts, B. J., Wingen, L. M., Sumner, A. L., Syomin, D., and Ramazan, K. A.: The heterogeneous hydrolysis of NO_2 in laboratory systems and in outdoor and indoor atmospheres: an integrated mechanism, Phys. Chem. Chem. Phys., 5, 223–242, https://doi.org/10.1039/b208564j, 2003.

Frey, M. M., Brough, N., France, J. L., Anderson, P. S., Traulle, O., King, M. D., Jones, A. E., Wolff, E. W., and Savarino, J.: The diurnal variability of atmospheric nitrogen oxides (NO and NO_2) above the Antarctic Plateau driven by atmospheric stability and snow emissions, Atmos. Chem. Phys., 13, 3045–3062, https://doi.org/10.5194/acp-13-3045-2013, 2013.

Frey, M. M., Roscoe, H. K., Kukui, A., Savarino, J., France, J. L., King, M. D., Legrand, M., and Preunkert, S.: Atmospheric nitrogen oxides (NO and NO_2) at Dome C, East Antarctica, during the OPALE campaign, Atmos. Chem. Phys., 15, 7859–7875, https://doi.org/10.5194/acp-15-7859-2015, 2015.

Fu, T.-M., Jacob, D. J., Wittrock, F., Burrows, J. P., Vrekoussis, M., and Henze, D. K.: Global budgets of atmospheric glyoxal and methylglyoxal, and implications for formation of secondary organic aerosols, J. Geophys. Res., 113, D15303, https://doi.org/10.1029/2007JD009505, 2008.

Fuchs, H., Dubé, W. P., Lerner, B. M., Wagner, N. L., Williams, E. J., and Brown, S. S.: A sensitive and versatile detector for atmospheric NO_2 and NO_x based on blue diode laser Cavity Ring-Down Spectroscopy, Environ. Sci. Technol., 43, 7831–7836, https://doi.org/10.1021/es902067h, 2009.

Fuchs, H., Ball, S. M., Bohn, B., Brauers, T., Cohen, R. C., Dorn, H.-P., Dubé, W. P., Fry, J. L., Häseler, R., Heitmann, U., Jones, R. L., Kleffmann, J., Mentel, T. F., Müsgen, P., Rohrer, F., Rollins, A. W., Ruth, A. A., Kiendler-Scharr, A., Schlosser, E., Shillings, A. J. L., Tillmann, R., Varma, R. M., Venables, D. S., Villena Tapia, G., Wahner, A., Wegener, R., Wooldridge, P. J., and Brown, S. S.: Intercomparison of measurements of NO_2 concentrations in the atmosphere simulation chamber SAPHIR during the NO3Comp campaign, Atmos. Meas. Tech., 3, 21–37, https://doi.org/10.5194/amt-3-21-2010, 2010.

Gherman, T., Venables, D. S., Vaughan, S., Orphal, J., and Ruth, A. A.: Incoherent Broadband Cavity-Enhanced Absorption Spectroscopy in the near-Ultraviolet: application to HONO and NO_2, Environ. Sci. Technol., 42, 890–895, https://doi.org/10.1021/es0716913, 2008.

Grilli, R., Méjean, G., Kassi, S., Ventrillard, I., Abd-Alrahman, C., Fasci, E., and Romanini, D.: Trace measurement of BrO at the ppt level by a transportable Mode-Locked Frequency-Doubled Cavity-Enhanced Spectrometer, Appl. Phys. B, 107, 205–212, https://doi.org/10.1007/s00340-011-4812-9, 2012.

Grosjean, D. and Harrison, J.: Response of chemiluminescence NO_x analyzers and ultraviolet ozone analyzers to organic air pollutants, Environ. Sci. Technol., 19, 862–865, https://doi.org/10.1021/es00139a016, 1985.

Heard, D. E.: High levels of the hydroxyl radical in the winter urban troposphere, Geophys. Res. Lett., 31, L18112, https://doi.org/10.1029/2004GL020544, 2004.

Jaworski, N. A., Howarth, R. W., and Hetling, L. J.: Atmospheric deposition of nitrogen oxides onto the landscape contributes to coastal eutrophication in the northeast United States, Environ. Sci. Technol., 31, 1995–2004, https://doi.org/10.1021/es960803f, 1997.

Jordan, N., Ye, C. Z., Ghosh, S., Washenfelder, R. A., Brown, S. S., and Osthoff, H. D.: A broadband cavity-enhanced spectrometer for atmospheric trace gas measurements and Rayleigh scattering cross sections in the cyan region (470–540 nm), Atmos. Meas. Tech., 12, 1277–1293, https://doi.org/10.5194/amt-12-1277-2019, 2019.

Kovalev, V. A. and Eichinger, W. E.: Elastic Lidar: theory, practice, and analysis methods, John Wiley & Sons, Inc., Hoboken, NJ, USA, https://doi.org/10.1002/0471643173, 2004.

Langridge, J. M., Ball, S. M., and Jones, R. L.: A compact Broadband Cavity Enhanced Absorption Spectrometer for detection of atmospheric NO_2 using light emitting diodes, Analyst, 131, 916–922, https://doi.org/10.1039/b605636a, 2006.

Lee, J. S., Kim, K.-H., Kim, Y. J., and Lee, J.: Application of a Long-Path Differential Optical Absorption Spectrometer (LP-DOAS) on the measurements of NO_2, SO_2, O_3, and HNO_2 in Gwangju, Korea, J. Environ. Manag., 86, 750–759, https://doi.org/10.1016/j.jenvman.2006.12.044, 2008.

Lee, J. S., Kim, Y. J., Kuk, B., Geyer, A., and Platt, U.: Simultaneous measurements of atmospheric pollutants and visibility with a Long-Path DOAS System in urban areas, Environ. Monit. Assess., 104, 281–293, https://doi.org/10.1007/s10661-005-1616-6, 2005.

Legrand, M., Preunkert, S., Frey, M., Bartels-Rausch, Th., Kukui, A., King, M. D., Savarino, J., Kerbrat, M., and Jourdain, B.: Large mixing ratios of atmospheric nitrous acid (HONO) at Concordia (East Antarctic Plateau) in summer: a strong source from surface snow?, Atmos. Chem. Phys., 14, 9963–9976, https://doi.org/10.5194/acp-14-9963-2014, 2014.

Leser, H., Hönninger, G., and Platt, U.: MAX-DOAS measurements of BrO and NO_2 in the marine boundary layer, Geophys. Res. Lett., 30, 1537–1541, https://doi.org/10.1029/2002GL015811, 2003.

Liang, S., Qin, M., Xie, P., Duan, J., Fang, W., He, Y., Xu, J., Liu, J., Li, X., Tang, K., Meng, F., Ye, K., Liu, J., and Liu, W.: Development of an incoherent broadband cavity-enhanced absorption spectrometer for measurements of ambient glyoxal and NO_2 in a polluted urban environment, Atmos. Meas. Tech., 12, 2499–2512, https://doi.org/10.5194/amt-12-2499-2019, 2019.

Liu, J., Li, X., Yang, Y., Wang, H., Wu, Y., Lu, X., Chen, M., Hu, J., Fan, X., Zeng, L., and Zhang, Y.: An IBBCEAS system for atmospheric measurements of glyoxal and methylglyoxal in the presence of high NO_2 concentrations, Atmos. Meas. Tech., 12, 4439–4453, https://doi.org/10.5194/amt-12-4439-2019, 2019.

Maeda, Y., Aoki, K., and Munemori, M.: Chemiluminescence method for the determination of nitrogen dioxide, Anal. Chem., 52, 307–311, https://doi.org/10.1021/ac50052a022, 1980.

Mauldin, R. L., Eisele, F. L., Tanner, D. J., Kosciuch, E., Shetter, R., Lefer, B., Hall, S. R., Nowak, J. B., Buhr, M., Chen, G., Wang,

P., and Davis, D.: Measurements of OH, H_2SO_4, and MSA at the South Pole during ISCAT, Geophys. Res. Lett., 28, 3629–3632, https://doi.org/10.1029/2000GL012711, 2001.

Min, K.-E., Washenfelder, R. A., Dubé, W. P., Langford, A. O., Edwards, P. M., Zarzana, K. J., Stutz, J., Lu, K., Rohrer, F., Zhang, Y., and Brown, S. S.: A broadband cavity enhanced absorption spectrometer for aircraft measurements of glyoxal, methylglyoxal, nitrous acid, nitrogen dioxide, and water vapor, Atmos. Meas. Tech., 9, 423–440, https://doi.org/10.5194/amt-9-423-2016, 2016.

Monks, P. S., Granier, C., Fuzzi, S., Stohl, A., Williams, M., Akimoto, H., Amann, M., Baklanov, A., Baltensperger, U., Bey, I., Blake, N., Blake, R., Carslaw, K., Cooper, O., Dentener, F., Fowler, D., Fragkou, E., Frost, G., Generoso, S., Ginoux, P., Grewe, V., Guenther, A., Hansson, H., Henne, S., Hjorth, J., Hofzumahaus, A., Huntrieser, H., Isaksen, I., Jenkin, M., Kaiser, J., Kanakidou, M., Klimont, Z., Kulmala, M., Laj, P., Lawrence, M., Lee, J., Liousse, C., Maione, M., McFiggans, G., Metzger, A., Mieville, A., Moussiopoulos, N., Orlando, J., O'Dowd, C., Palmer, P., Parrish, D., Petzold, A., Platt, U., Pöschl, U., Prévôt, A., Reeves, C., Reimann, S., Rudich, Y., Sellegri, K., Steinbrecher, R., Simpson, D., ten Brink, H., Theloke, J., van der Werf, G., Vautard, R., Vestreng, V., Vlachokostas, C., and von Glasow, R.: Atmospheric composition change – global and regional air quality, Atmos. Environ., 43, 5268–5350, https://doi.org/10.1016/j.atmosenv.2009.08.021, 2009.

Monks, P. S.: Gas-phase radical chemistry in the troposphere, Chem. Soc. Rev., 34, 376, https://doi.org/10.1039/b307982c, 2005.

Pikelnaya, O., Hurlock, S. C., Trick, S., and Stutz, J.: Intercomparison of MultiAXis and Long-Path Differential Optical Absorption Spectroscopy measurements in the marine boundary layer, J. Geophys. Res.-Atmos., 112, D10S01, https://doi.org/10.1029/2006JD007727, 2007.

Platt, U. and Perner, D.: Direct measurements of atmospheric CH_2O, HNO_2, O_3, NO_2, and SO_2 by Differential Optical Absorption in the near UV, J. Geophys. Res.-Oceans, 85, 7453–7458, https://doi.org/10.1029/JC085iC12p07453, 1980.

Pöhler, D., Vogel, L., Friess, U., and Platt, U.: Observation of halogen species in the Amundsen Gulf, Arctic, by active Long-Path Differential Optical Absorption Spectroscopy, P. Natl. Acad. Sci. USA, 107, 6582–6587, https://doi.org/10.1073/pnas.0912231107, 2010.

Richard, L., Romanini, D., and Ventrillard, I.: Nitric oxide analysis down to ppt levels by Optical-Feedback Cavity-Enhanced Absorption Spectroscopy, Sensors, 18, 1997, https://doi.org/10.3390/s18071997, 2018.

Rozanov, V. V. and Rozanov, A. V.: Differential optical absorption spectroscopy (DOAS) and air mass factor concept for a multiply scattering vertically inhomogeneous medium: theoretical consideration, Atmos. Meas. Tech., 3, 751–780, https://doi.org/10.5194/amt-3-751-2010, 2010.

Ruth, A. A., Dixneuf, S., and Raghunandan, R.: Broadband Cavity-Enhanced Absorption Spectroscopy with Incoherent Light, in: Cavity-Enhanced Spectroscopy and Sensing, edited by: Gagliardi, G. and Loock, H.-P., Springer Berlin Heidelberg, Berlin, Heidelberg, 179, 485–517, https://doi.org/10.1007/978-3-642-40003-2_14, 2014.

Ryerson, T. B., Williams, E. J., and Fehsenfeld, F. C.: An efficient photolysis system for fast-response NO_2 measurements, J. Geophys. Res.-Atmos., 105, 26447–26461, https://doi.org/10.1029/2000JD900389, 2000.

Sinreich, R., Volkamer, R., Filsinger, F., Frieß, U., Kern, C., Platt, U., Sebastián, O., and Wagner, T.: MAX-DOAS detection of glyoxal during ICARTT 2004, Atmos. Chem. Phys., 7, 1293–1303, https://doi.org/10.5194/acp-7-1293-2007, 2007.

Thalman, R. and Volkamer, R.: Inherent calibration of a blue LED-CE-DOAS instrument to measure iodine oxide, glyoxal, methyl glyoxal, nitrogen dioxide, water vapour and aerosol extinction in open cavity mode, Atmos. Meas. Tech., 3, 1797–1814, https://doi.org/10.5194/amt-3-1797-2010, 2010.

Triki, M., Cermak, P., Méjean, G., and Romanini, D.: Cavity-Enhanced Absorption Spectroscopy with a red LED source for NO_x trace analysis, Appl. Phys. B, 91, 195–201, https://doi.org/10.1007/s00340-008-2958-x, 2008.

Vandaele, A., Hermans, C., Simon, P., Carleer, M., Colin, R., Fally, S., Mérienne, M., Jenouvrier, A., and Coquart, B.: Measurements of the NO_2 absorption cross-section from 42 000 cm^{-1} to 10 000 cm^{-1} (238–1000 nm) at 220 K and 294 K, J. Quant. Spectrosc. Ra., 59, 171–184, https://doi.org/10.1016/S0022-4073(97)00168-4, 1998.

Venables, D. S., Gherman, T., Orphal, J., Wenger, J. C., and Ruth, A. A.: High sensitivity in situ monitoring of NO_3 in an atmospheric simulation chamber using Incoherent Broadband Cavity-Enhanced Absorption Spectroscopy, Environ. Sci. Technol., 40, 6758–6763, https://doi.org/10.1021/es061076j, 2006.

Ventrillard-Courtillot, I., Sciamma O'Brien, E., Kassi, S., Méjean, G., and Romanini, D.: Incoherent Broad-Band Cavity-Enhanced Absorption Spectroscopy for simultaneous trace measurements of NO_2 and NO_3 with a LED source, Appl. Phys. B, 101, 661–669, https://doi.org/10.1007/s00340-010-4253-x, 2010.

Villena, G., Bejan, I., Kurtenbach, R., Wiesen, P., and Kleffmann, J.: Interferences of commercial NO2 instruments in the urban atmosphere and in a smog chamber, Atmos. Meas. Tech., 5, 149–159, https://doi.org/10.5194/amt-5-149-2012, 2012.

Vitousek, P. M., Aber, J. D., Howarth, R. W., Likens, G. E., Matson, P. A., Schindler, D. W., Schlesinger, W. H., and Tilman, D. G.: Human alteration of the global nitrogen cycle: sources and consequences, Ecol. Appl., 7, 737–750, https://doi.org/10.1890/1051-0761(1997)007[0737:HAOTGN]2.0.CO;2, 1997.

Volkamer, R., Spietz, P., Burrows, J., and Platt, U.: High-resolution absorption cross-section of glyoxal in the UV–vis and IR spectral ranges, J. Photoch. Photobio. A, 172, 35–46, https://doi.org/10.1016/j.jphotochem.2004.11.011, 2005.

Volkamer, R., San Martini, F., Molina, L. T., Salcedo, D., Jimenez, J. L., and Molina, M. J.: A missing sink for gas-phase glyoxal in Mexico City: formation of secondary organic aerosol, Geophys. Res. Lett., 34, L19807, https://doi.org/10.1029/2007GL030752, 2007.

Wachsstock, D.: Tenua: the kinetics simulator for Java, available at: http://bililite.com/tenua (last access: 7 May 2020), 2007.

Wagner, T., Ibrahim, O., Shaiganfar, R., and Platt, U.: Mobile MAX-DOAS observations of tropospheric trace gases, Atmos. Meas. Tech., 3, 129–140, https://doi.org/10.5194/amt-3-129-2010, 2010.

Washenfelder, R. A., Langford, A. O., Fuchs, H., and Brown, S. S.: Measurement of glyoxal using an incoherent broadband cav-

ity enhanced absorption spectrometer, Atmos. Chem. Phys., 8, 7779–7793, https://doi.org/10.5194/acp-8-7779-2008, 2008.

Werle, P., Mücke, R., and Slemr, F.: The limits of signal averaging in atmospheric trace-gas monitoring by Tunable Diode-Laser Absorption Spectroscopy (TDLAS), Appl. Phys. B, 57, 131–139, https://doi.org/10.1007/BF00425997, 1993.

Williams, E. J., Baumann, K., Roberts, J. M., Bertman, S. B., Norton, R. B., Fehsenfeld, F. C., Springston, S. R., Nunnermacker, L. J., Newman, L., Olszyna, K., Meagher, J., Hartsell, B., Edgerton, E., Pearson, J. R., and Rodgers, M. O.: Intercomparison of ground-based NO_y measurement techniques, J. Geophys. Res.-Atmos., 103, 22261–22280, https://doi.org/10.1029/98JD00074, 1998.

Wine, P. H. and Nicovich, J. M.: Atmospheric Radical Chemistry, in: Encyclopedia of Radicals in Chemistry, Biology and Materials, edited by: Chatgilialoglu, C. and Studer, A., John Wiley & Sons, Ltd, Chichester, UK, https://doi.org/10.1002/9781119953678.rad015, 2012.

Wittrock, F., Oetjen, H., Richter, A., Fietkau, S., Medeke, T., Rozanov, A., and Burrows, J. P.: MAX-DOAS measurements of atmospheric trace gases in Ny-Ålesund – Radiative transfer studies and their application, Atmos. Chem. Phys., 4, 955–966, https://doi.org/10.5194/acp-4-955-2004, 2004.